Charge-transfer cross sections in collisions of ground-state Ca and H^+

C. M. Dutta,[1] C. Oubre,[1] P. Nordlander,[1] M. Kimura,[2] and A. Dalgarno[3]
[1]*Department of Physics and Rice Quantum Institute, Rice University, Houston, Texas 77251-1892, USA*
[2]*Graduate School of Sciences, Kyushu University, Hakozaki, Fukuoka 812-8581, Japan*
[3]*Harvard-Smithsonian Center for Astrophysics, Cambridge, Massachusetts 02138 USA*
(Received 19 July 2005; revised manuscript received 19 December 2005; published 15 March 2006)

We have investigated collisions of $Ca(4s^2)$ with H^+ in the energy range of 200 eV/u–10 keV/u using the semiclassical molecular-orbital close-coupling (MOCC) method with 18 coupled molecular states (11 $^1\Sigma^+$ and seven $^1\Pi^+$ states) to determine charge-transfer cross sections. Except for the incoming channel 6 $^1\Sigma^+$, the molecular states all correspond to charge-transfer channels. Inclusion of Ca^{2+}-H^- is crucial in the configuration-interaction calculation for generating the molecular wave functions and potentials. Because of the Coulomb attraction, the state separating to Ca^{2+}-H^- creates many avoided crossings, even though at infinite separation it lies energetically above all other states that we included. Because of the avoided crossings between the incoming channel 6 $^1\Sigma^+$ and the energetically close charge-transfer channel 7 $^1\Sigma^+$ the charge-transfer interaction occurs at long range. This makes calculations of charge-transfer cross sections by the MOCC method very challenging. The total charge-transfer cross sections increase monotonically from 3.4×10^{-15} cm^2 at 200 eV/u to 4.5×10^{-15} cm^2 at 10 keV/u. Charge transfer occurs mostly to the excited $Ca^+(5p)$ state in the entire energy range, which is the sum of the charge transfer to 7 $^1\Sigma^+$ and 4 $^1\Pi^+$. It accounts for ~47% of the total charge transfer cross sections at 200 eV/u. However, as the energy increases, transfer to $Ca^+(4d)$ increases, and at 10 keV/u the charge-transfer cross sections for $Ca^+(5p)$ and $Ca^+(4d)$ become comparable, each giving ~38% of the total cross section.

DOI: 10.1103/PhysRevA.73.032714 PACS number(s): 34.10.+x, 34.70.+e, 34.60.+z

I. INTRODUCTION

Calcium is one of the major atomic species in the interstellar medium and observations of the Ca^+ spectral lines have been made to map the distribution of interstellar clouds [1–3]. In diffuse clouds and at the edges of dense clouds, the calcium atom is singly ionized because its ionization potential of 6.111 eV is smaller than that of hydrogen. Deeper into the clouds, the dominant configuration is neutral Ca. The distribution of calcium in its ionized and neutral states is important for abundance determinations. Calcium atoms are also relatively abundant in biological systems, and the interactions of calcium atoms and ions with protons and hydrogen atoms are important in proton and heavy-ion beam therapy and in diagnostic applications. Collisions of $Ca^+(4s)$, $Ca^+(3d)$, and $Ca^+(4p)$ ions with hydrogen atoms have been studied previously [4–9], but there has been no published work to our knowledge on charge transfer between calcium atoms and hydrogen ions, neither theoretical nor experimental. In this paper we present a theoretical investigation of the charge transfer of ground-state Ca atoms colliding with protons at collision energies between 200 eV/u and 10 keV/u.

II. THEORY

The process we consider is

$$\mathrm{Ca}(4s^2) + \mathrm{H}^+ \rightarrow \mathrm{Ca}^+ + H(1s). \tag{1}$$

We apply the molecular-orbital close-coupling (MOCC) method, within the semiclassical impact-parameter approximation. The method is explained in detail by Kimura and Thorson [10]. The electron translation factors are expanded in collision velocity $\vec{v}$, and terms are kept up to the first order in $\vec{v}$. In [10], He^{2+}-$H(1s)$ collisions were studied, and it was found that at keV energies, the contributions from the terms of second order in $\vec{v}$ changed the results by at most 1%. The effect of higher orders of $\vec{v}$ is expected to be at most a few percent in the low-keV region. The molecular orbitals are represented by linear combinations of Slater orbitals. The interactions of the Ca^{2+} core electrons are replaced by the pseudopotential

$$V(\vec{r}) = \sum_{l,m} A_l \exp(-\xi r^2)|l,m\rangle\langle l,m| - \frac{\alpha_d}{2(r^2+d^2)^2} - \frac{\alpha_q}{2(r^2+d^2)^3} - \frac{Z_{eff}}{r} \tag{2}$$

used earlier for Li^++Ca collisions [11,12]. The parameters are listed in these papers. To obtain better agreement between the experimental and calculated energies of the higher excited states, the parameter A_0 in [12] was slightly changed from 14.657 839 to 12.320 839, while the other parameters were kept the same. The adiabatic potentials and wave functions were obtained by configuration interaction (CI) calculations including single and double excitations and also Ca^{2+}-$H^-(1s1s')$ configurations, where $1s$ and $1s'$ are Slater orbitals. To find the optimum set of Slater exponents, we used a genetic selection-type code [13] written by one of the authors (C.O.). In this approach, we started with a large number of sets of randomly selected Slater exponents, and carried out CI calculations to obtain molecular-state energies at a large internuclear separation $R=30$ a.u. Then, the energy of each set was evaluated and assigned a score based on the degree

TABLE I. Molecular states, asymptotic configurations, and calculated and measured energies.

Molecular state	Asymptotic configuration	Calculated energy (a.u.)	Measured energy (a.u.)
$1\ ^1\Sigma^+$	$Ca^+(4s)+H(1s)$	−0.9504	−0.9362
$2\ ^1\Sigma^+$	$Ca^+(3d)+H(1s)$	−0.8732	−0.8738
$1\ ^1\Pi^+$			
$3\ ^1\Sigma^+$	$Ca^+(4p)+H(1s)$	−0.8197	−0.8209
$2\ ^1\Pi^+$			
$4\ ^1\Sigma^+$	$Ca^+(5s)+H(1s)$	−0.7030	−0.6985
$5\ ^1\Sigma^+$	$Ca^+(4d)+H(1s)$	−0.6767	−0.6772
$3\ ^1\Pi^+$			
$6\ ^1\Sigma^+$	$Ca(4s^2)+H^+$	−0.6599	−0.6608
$7\ ^1\Sigma^+$	$Ca^+(5p)+H(1s)$	−0.6595	−0.6602
$4\ ^1\Pi^+$			
$8\ ^1\Sigma^+$	$Ca^+(4f)+H(1s)$	−0.6255	−0.6261
$5\ ^1\Pi^+$			
$9\ ^1\Sigma^+$	$Ca^+(6s)+H(1s)$	−0.6142	−0.6142
$10\ ^1\Sigma^+$	$Ca^+(5d)+H(1s)$	−0.6041	−0.6048
$6\ ^1\Pi^+$			
$11\ ^1\Sigma^+$	$Ca^+(6p)+H(1s)$	−0.5962	−0.5967
$7\ ^1\Pi^+$			

of deviation of the calculated molecular-state energies from the measured atomic energies. The sets with higher scores as measured by the better agreement of the molecular-state energies with experiment are allowed to "breed" more often. The breeding generates a new collection of sets of Slater orbitals. The process repeats until the sets stabilize and the deviations of energies are within our acceptable values. We cannot overemphasize the importance of including the Ca^{2+}-$H^-(1s1s')$ configurations. When these configurations were excluded, many avoided crossings, crucial to charge transfer, disappeared, and the exponents of the Slater type orbitals (STO's) drastically changed.

III. RESULTS

The energy levels of the lowest 11 $^1\Sigma^+$ and seven $^1\Pi^+$ molecular orbitals calculated at $R=30$ a.u. are compared with experimentally observed energy levels [14] of the separated ion-atom systems in Table I. Since the measured ionization potentials are known to four effective digits, we list the energy to four effective digits. In comparing the calculated molecular-state energies with the observed ones, we took the weighted average of the energy levels of different J values. This averaging does not affect the first three digits. The deviations of the calculated energies from the measurements are less than 1%, except for the $1\ ^1\Sigma^+$ state for which the deviation is 1.5%. However, we note that the energy gap between the $6\ ^1\Sigma^+$ and $7\ ^1\Sigma^+$ occurs at the fourth decimal point, and the J multiplicity splitting of the $7\ ^1\Sigma^+$ state, which separates to $Ca^+(5p)$ and $H(1s)$ at large R, is 0.000 36 a.u. Table II shows the Slater orbitals and optimized exponents used in the present calculations. At the hydrogen site the exponents of $2s$ STO's are larger than those for $1s$ STO's. This is unusual. This is due to inclusion of the Ca^{2+}-H^- configurations. When we carried out the optimization using the same code [13] without the Ca^{2+}-H^- configurations, this unusual feature was not observed. For example, the exponents for the $1s$ STO at the hydrogen site were 2.0000, 1.0000, and 0.500 00, while the exponents for the $2s$ STO were 1.649 20, and 0.737 60, respectively. Similarly, the exponents of STO's for higher excited states at the Ca site showed more regular trends as we would expect. Also when the Ca^{2+}-H^- configurations were excluded, there were few avoided crossings in the Σ state potentials. When we included the Ca^{2+}-H^- configurations and started optimization with the same initial values as the STO exponent values obtained from the previous calculation without the Ca^{2+}-H^- configurations, we obtained the set of STO exponents shown in Table II. Therefore, the large exponents of $2s$ STO's as well as considerable changes in other exponents and the numerous avoided crossings seen in Fig. 1(a) are due to inclusion of the Ca^{2+}-H^- configurations. Because of the strong Coulomb attraction, the state separating to Ca^{2+}-H^- creates many avoided crossings, even though at infinite separation it lies energetically above the other states that we included. The set of STO exponents that minimizes the energy differences

TABLE II. Slater orbitals and optimized exponents.

Site	STO	Exponent	STO	Exponent
H site	$1s$	1.0856	$2p$	0.6532
		0.2116		3.0772
		0.5788		2.3600
	$2s$	3.9688		
		3.7760		
Ca site	$4s$	1.1588		
		1.3800		
		0.2712		
		0.6280		
		1.8080		
		0.6000		
	$4p$	0.9052	$3d$	0.2348
		0.5160		1.5328
		0.7228		
	$5s$	0.0560	$4d$	3.5364
		2.2108		3.0192
				0.6912
	$5p$	1.0176	$4f$	0.4380
		0.3156		0.3636
		3.6480		0.4112
	$5d$	1.0104		
		0.5236		
	$6s$	0.2850		
		0.7992		
	$6p$	2.1944		
		0.5196		

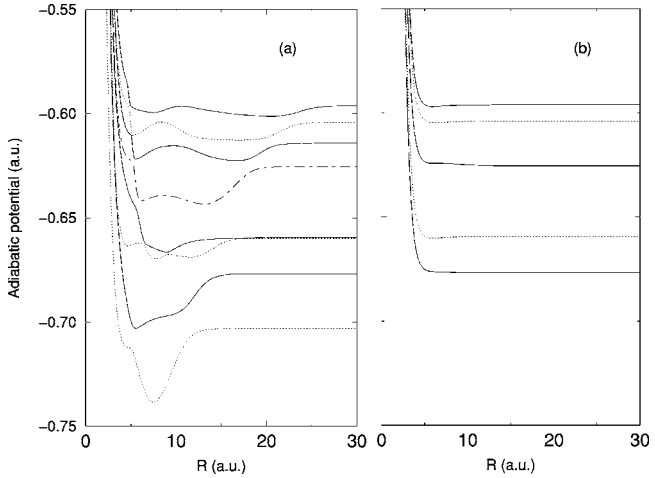

FIG. 1. Adiabatic potentials of the CaH^+ molecule. (a) The $n\ ^1\Sigma^+$ states from $n=4$ at the bottom to $n=11$ at the top, and (b) the $n\ ^1\Pi^+$ states from $n=3$ at the bottom to $n=7$ at the top. The order of the states is as shown in Table I.

between the observed and calculated molecular-state energies at large internuclear separations R (we chose $R=30$ a.u.) may not be unique and the coefficients of the individual CI determinants depend on the given set of optimized STO's. However, we believe that in spite of the lack of uniqueness of the optimized STO's, the wave functions and potentials we obtained are still physically meaningful.

In order to examine our wave functions and potentials, we compare our results with other calculated potentials and dissociation energies. Unfortunately, most molecular-orbital calculations were carried out in the region of small R, less than $\sim$10 a.u., and also only for relatively low-lying states. Kerkeni *et al.* [15] calculated the $1\ ^1\Sigma^+$, $2\ ^1\Sigma^+$, and $3\ ^1\Sigma^+$ state potentials. These three states appear to agree well with their results, which are presented graphically for R up to 14 a.u. in their paper. Boutalib *et al.* [16] calculated the lowest four $^1\Sigma^+$ states and the lowest $^1\Pi^+$ state. The state potentials shown in Fig. 4 of their paper compare well with ours. They also compared their calculated equilibrium distances R_e and the dissociation energies, D_e, of these states with other calculations. We show our calculated R_e and D_e in Table III. The values agree well with those given in Tables 3 and 4 in [16] except that of $1\ ^1\Pi^+$. Our D_e for this state is smaller. However, for charge transfer the contribution from the $1\ ^1\Pi^+$ state is negligible. The lowest four $1\ ^1\Sigma^+$ states and the lowest $^1\Pi^+$ state have shallow wells listed in Table III indicating that a stable ground state of the CaH^+ molecule exists. In the present case, the important molecular states are higher excited states, and there are no theoretical or measured data available for comparison. The entrance channel that separates to H^+ and $Ca(4s^2)$ is the $6\ ^1\Sigma^+$ state. All the other states are charge-transfer states. Among the eighteen states we coupled, the pairs of $[1\ ^1\Pi^+, 2\ ^1\Sigma^+]$, $[2\ ^1\Pi^+, 3\ ^1\Sigma^+]$, $[3\ ^1\Pi^+, 5\ ^1\Sigma^+]$, $[4\ ^1\Pi^+, 7\ ^1\Sigma^+]$, $[5\ ^1\Pi^+, 8\ ^1\Sigma^+]$, $[6\ ^1\Pi^+, 10\ ^1\Sigma^+]$, and $[7\ ^1\Pi^+, 11\ ^1\Sigma^+]$ states are asymptotically degenerate.

TABLE III. The equilibrium distance and the dissociation energy of the lowest four $^1\Sigma^+$ and $1\ ^1\Pi^+$ states.

Molecular states	Equilibrium distance (a.u.)	Dissociation energy (eV)
$1\ ^1\Sigma^+$	3.45	1.906
$2\ ^1\Sigma^+$	4.20	0.906
$3\ ^1\Sigma^+$	5.35	0.838
$1\ ^1\Pi^+$	7.49	0.971
$1\ ^1\Pi^+$	6.55	0.017

The cross sections were calculated using the straight line trajectory impact parameter method. The partial cross section is obtained from

$$\sigma_{f,i} = 2\pi \int_{b_{min}}^{b_{max}} P_{f,i}(b) b\, db \tag{3}$$

where i and f denote the initial and final channels, respectively, b is the impact parameter, and $P_{f,i}(b)$ is the transition probability for b. The limits b_{min} and b_{max} are zero and ∞, respectively. In practice, b_{min} cannot be chosen to be zero, since the use of the pseudopotential for the core electrons of Ca prevents us from obtaining accurate wave functions at small R. We took b_{min} equal to 2.2 a.u. The upper limit b_{max} was taken large enough that the transition probability becomes zero. Our cross sections do not include the contribution from $b<b_{min}$, and thus give lower limits.

The potential energy curves are shown in Figs. 1(a) and 1(b). Figure 1(a) shows eight $^1\Sigma^+$ states. The three lowest $^1\Sigma^+$ states lie below the energy scale. Figure 1(b) shows five $^1\Pi^+$ states. The two lowest $^1\Pi^+$ states lie below the energy scale. We observe many avoided level crossings between higher excited $^1\Sigma^+$ states. The positions and energy gaps of the avoided crossings are listed in Table IV. The energy gaps at very small R (<3 a.u.) may be less accurate because of use of the pseudopotential. These avoided crossings disappear if we do not include Ca^{2+}-H^- configurations in the CI calculation. The energy of the Ca^{2+}-H^- system at large R is $-0.125\ 35$ a.u., and there exist many excited Ca^+ and $H(1s)$ energy levels between this energy and the highest Σ^+ state energy we included here. However, inclusion of the Ca^{2+}-H^- configurations has an important influence on the Σ^+ states. The avoided crossings at $R \gg R_{pol}$ where the polarization potentials become negligible are caused by the exchange interactions, and the energy gap should exponentially decrease with increasing R [19]. In the present case, the energy gap at the avoided crossings at R beyond $\sim$15 a.u. is caused by the exchange interactions. The position of the avoided crossing should increase for higher MO's, since R_{pol} is inversely proportional to the MO energy. Therefore, we expect that higher molecular states have larger values of R_{pol}. This is consistent with the increasingly long-range avoided crossings between $9\ ^1\Sigma^+$ and $8\ ^1\Sigma^+$, $10\ ^1\Sigma^+$ and $9\ ^1\Sigma^+$, and $11\ ^1\Sigma^+$ and $10\ ^1\Sigma^+$ seen in Table IV. We also expect the energy gaps for these to be of the order of 10^{-5} or smaller using the method described in [19], but in Table IV these gaps are of the order of 10^{-3}. This indicates that these four higher excited $^1\Sigma^+$ states are less accurate at large R than the lower

TABLE IV. Positions of the avoided crossings (R) and the corresponding energy gaps among molecular states shown in Table I.

Molecular state	R (a.u.)	Energy gap (a.u.)
$5\ ^1\Sigma^+$–$4\ ^1\Sigma^+$	5.16	1.244×10^{-2}
	11.33	1.675×10^{-2}
$6\ ^1\Sigma^+$–$5\ ^1\Sigma^+$	3.32	3.826×10^{-3}
	8.00	2.844×10^{-2}
$7\ ^1\Sigma^+$–$6\ ^1\Sigma^+$	2.46	1.936×10^{-2}
	6.49	1.344×10^{-3}
	9.07	1.151×10^{-3}
	17.23	2.300×10^{-5}
$8\ ^1\Sigma^+$–$7\ ^1\Sigma^+$	3.42	4.374×10^{-3}
	5.73	8.721×10^{-3}
	13.37	1.697×10^{-2}
$9\ ^1\Sigma^+$–$8\ ^1\Sigma^+$	5.27	4.409×10^{-3}
	18.46	6.493×10^{-3}
$10\ ^1\Sigma^+$–$9\ ^1\Sigma^+$	3.01	1.583×10^{-3}
	5.06	3.284×10^{-3}
	11.57	6.499×10^{-3}
	20.43	5.277×10^{-3}
$11\ ^1\Sigma^+$–$10\ ^1\Sigma^+$	4.80	4.731×10^{-3}
	8.02	4.874×10^{-3}
	23.09	5.786×10^{-3}

states. This may be partly due to the pseudopotential we used, but also because the effect of the incompleteness of the STO basis set is more severe for these excited states. However, the contributions from these very highly excited states to the total charge-transfer cross sections were found to be relatively small ($\sim$9%).

The entrance channel is the $6\ ^1\Sigma^+$ state that separates to $Ca(4s^2)$ and H^+ at large R. All the other channels are populated by charge transfer. In Fig. 2(a), we magnify the potentials of the incoming channel $6\ ^1\Sigma^+$ and $7\ ^1\Sigma^+$ near the avoided crossings, since these two channels are most important in charge transfer. Our CI code gives the correct relative phases of the molecular orbitals at each R, but not the absolute phases. Therefore, in calculating the radial and rotational coupling matrix elements we need to select signs of all the phases of the molecular orbitals at each R, so that the wave functions vary smoothly with R, and consequently produce smooth coupling matrix elements. Figure 2(b) shows the radial coupling matrix elements between $7\ ^1\Sigma^+$ and $6\ ^1\Sigma^+$. They are large near the avoided crossings, and the height of the peak is higher and the width of the peak is narrower when the energy gap at the crossing is smaller. From Fig. 1, we expect charge transfer to the $7\ ^1\Sigma^+$ state to be most probable. Since the $4\ ^1\Pi^+$ state is degenerate with $7\ ^1\Sigma^+$ at large R and also directly coupled with the incoming $6\ ^1\Sigma^+$ state, we also expect charge transfer to the $4\ ^1\Pi^+$ state to be sizable. There are other large radial coupling matrix elements, especially at the avoided crossings, among other higher Σ^+ states. As mentioned earlier the four highest $^1\Sigma^+$ are less accurate. However, they are much above the incoming channel, and since they are all charge-transfer states, we expect

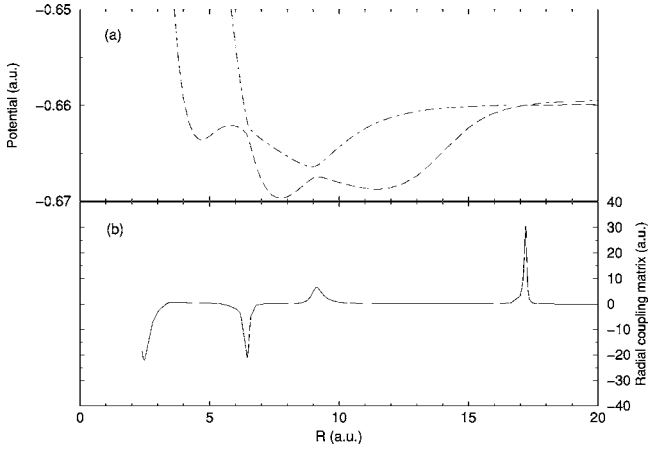

FIG. 2. (a) Magnified potential curves for $6\ ^1\Sigma^+$ (long-dashed curve), $7\ ^1\Sigma^+$ (dot-dashed curve), and diabatic potential curves for $6\ ^1\Sigma^+_{dia}$ (dotted curve), $7\ ^1\Sigma^+_{dia}$ (solid curve). The diabatic potentials cross each other. (b) Radial coupling matrix element between $7\ ^1\Sigma^+$ and $6\ ^1\Sigma^+$.

that the net contribution to charge transfer is largely independent of the individual coupling matrix elements and the energy gaps among them. Also, since the contributions from the states from $8\ ^1\Sigma^+$ and above were less than 9% of the total charge-transfer cross sections, this will not significantly change the magnitude of the total cross sections. Figures 3(a) and 3(b), respectively, show some relatively large radial and rotational coupling matrix elements coupled with the incoming $6\ ^1\Sigma^+$ state. In Fig. 3(b), we also included the rotational coupling matrix elements between $4\ ^1\Pi^+$ and $7\ ^1\Sigma^+$ which are degenerate at large R.

Figure 4 shows the partial charge-transfer cross sections leading to various Ca^+ ions, together with the total charge-transfer cross sections. We used the adiabatic potentials and coupling matrix elements in calculating these cross sections.

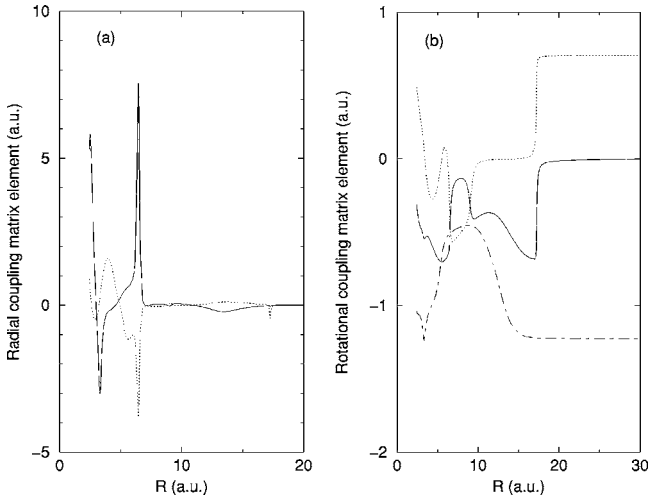

FIG. 3. Examples of the coupling matrix elements. (a) Radial coupling matrix elements: solid line, $5\ ^1\Sigma^+$–$6\ ^1\Sigma^+$; dotted line, $8\ ^1\Sigma^+$–$6\ ^1\Sigma^+$. (b) Rotational coupling matrix elements: solid line, $3\ ^1\Pi^+$–$6\ ^1\Sigma^+$; dotted line, $4\ ^1\Pi^+$–$7\ ^1\Sigma^+$; dot-dashed line, $4\ ^1\Pi^+$–$6\ ^1\Sigma^+$.

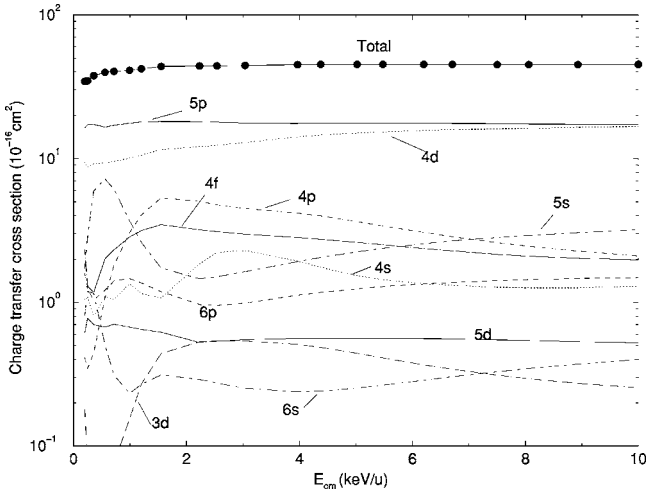

FIG. 4. Total and partial charge-transfer cross sections. Total charge-transfer cross section, line with circles, and the labeling of each curve indicates the final products of $Ca^+(nl)$ ions. The partial cross sections of the degenerate states were added to give the cross sections for $Ca^+(nl)$.

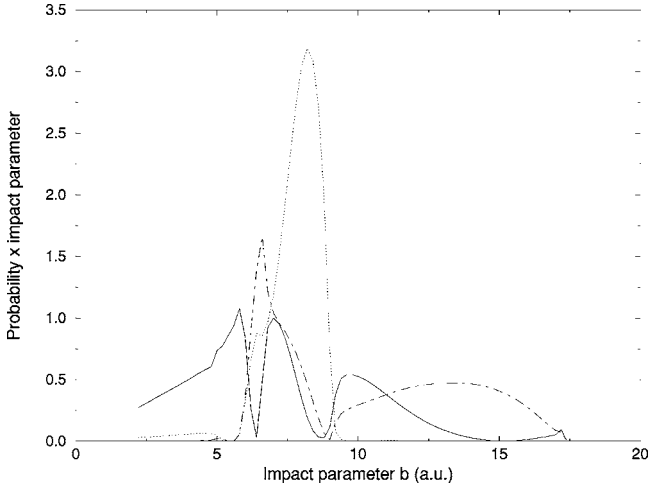

FIG. 5. Product of probability and impact parameter versus impact parameter for the 7 $^1\Sigma^+$ (full line), 5 $^1\Sigma^+$ (dotted line), and 4 $^1\Pi^+$ (dot-dashed line) states. The collision energy is 2.232 keV/u (the velocity 0.3 a.u.)

In this figure, the partial cross sections of the degenerate states (see Table I) are summed. For example, the partial cross section curve marked "5*p*" is the sum of the partial of 7 $^1\Sigma^+$ and 4 $^1\Pi$. In this case, the 7 $^1\Sigma^+$ and the 4 $^1\Pi$ cross sections are nearly equal in magnitude in the entire energy range. The total charge-transfer cross sections increase monotonically with energy, from 3.4×10^{-15} cm^2 at 200 eV/u to 4.5×10^{-15} cm^2 at 10 keV/u. As shown in Fig. 4, the dominant transfer in the entire energy range is to the 7 $^1\Sigma^+$ state and the 4 $^1\Pi^+$ states, together leading to $Ca^+(5p)$ production ($\sim$47% of the total charge-transfer cross section at the lowest energy, and $\sim$38% at 10 keV/u, respectively). The next large contribution to the charge transfer leads to $Ca^+(4d)$ production. This is the sum of the partial cross sections of the 5 $^1\Sigma^+$ and its degenerate 3 $^1\Pi^+$ state. These two states lie energetically just below the entrance channel. Charge transfer to $Ca^+(4d)$ increases with the collision energy and at 10 keV/u, it is as large as transfer to $Ca^+(5p)$, each channel contributing $\sim$38% to the total cross section. At the lower end of the collision energies, transfer to 4 $^1\Sigma^+$ peaks near 5.8 eV/u, because of the shallow well of the state at $R\sim7.4$ a.u. If we exclude contributions from R less than 10 a.u., the peak disappears. From this figure, we conjecture that at low eV energies, the three-state coupling of 6 $^1\Sigma^+$, 7 $^1\Sigma^+$ and 4 $^1\Pi^+$ will suffice to yield most of the total charge-transfer cross sections. The higher excited states leading to production of $Ca^+(6s)$, $Ca^+(5d)$, and $Ca^+(6p)$ give net contributions of less than 9% in the entire energy range.

Figure 5 plots the products of the probability and the impact parameter, $bP(b)$, versus b at 2.232 keV/u ($v=0.3$ a.u.) as an example. Because of the sharp peak in the radial coupling matrix elements and the extremely narrow energy gap between 6 $^1\Sigma^+$ and 7 $^1\Sigma^+$ that occurs at $R=17.23$ a.u. (see Fig. 2), we expected that most of the charge transfer to 7 $^1\Sigma^+$, and subsequently 4 $^1\Pi^+$, would occur here, and charge transfer in the present system is a long-range phenomenon, in contrast to the short range found in most charge transfer. Therefore, we calculated the partial charge transfer cross sections, increasing b_{min} so that these coupling peaks in Fig. 2(b) are avoided except the peak at $R=17.23$ a.u., for the case of $v=0.3$ a.u. We found that when we chose $b_{min}=10$ a.u., the partial cross sections of 7 $^1\Sigma^+$ and 4 $^1\Pi^+$ yielded 47% and 70%, respectively, of the corresponding partial cross sections that included all the peaks in Fig. 2(b). The 4 $^1\Pi^+$ partial cross sections are indirectly affected by the avoided crossing and the radial coupling matrix elements between 6 $^1\Sigma^+$ and 7 $^1\Sigma^+$.

In Fig. 6(a), we plot the time evolution of the probability of populating 7 $^1\Sigma^+$ by a solid line at the impact parameter $b=5$ a.u., and $v=0.3$ a.u. The collision starts at $t=-\infty$, and the probability rapidly increases at $t\sim-55$ a.u. ($R\sim17$ a.u.), stays stationary, and then oscillates rapidly up

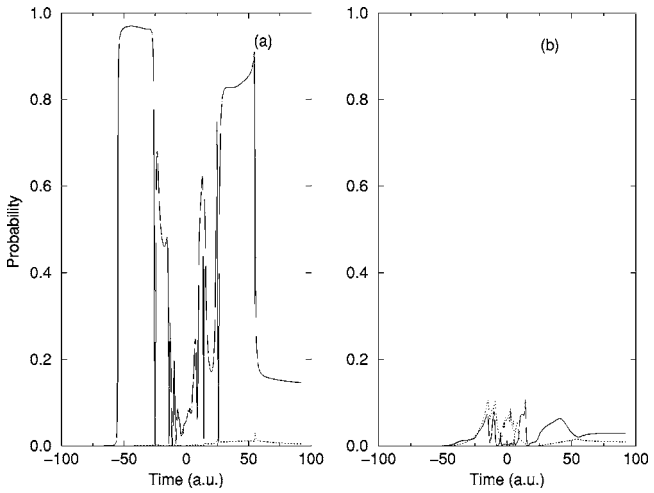

FIG. 6. (a) Time evolution of the 7 $^1\Sigma^+$ probability ($v=0.3$ a.u. and $b=0.5$ a.u.) using the adiabatic basis set. The dotted line is for 4 $^1\Pi^+$. (b) The same as in (a), using the diabatic basis set.

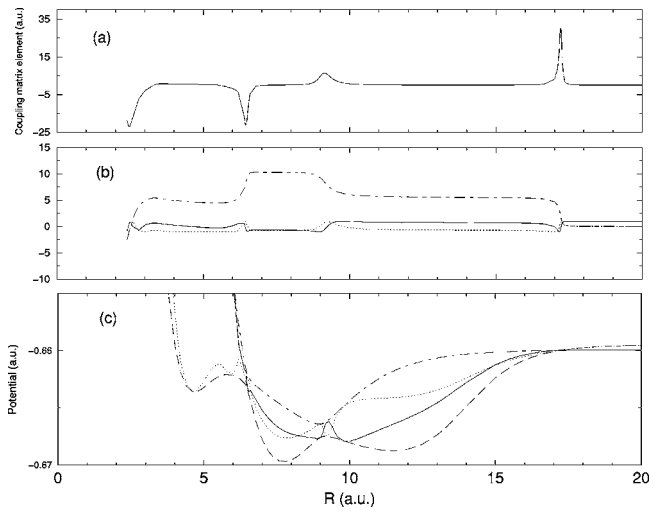

FIG. 7. (a) Radial coupling between 7 $^1\Sigma^+$ and 6 $^1\Sigma^+$ used for obtaining $\omega(R)$. (b) $\omega(R)$ (solid line), $\sin\omega(R)$ (dotted line), and $\cos\omega(R)$ (dot-dashed line). (c) The diabatic potentials for 6 $^1\Sigma^+$ (full line) and 7 $^1\Sigma^+$ (dotted line). They are enveloped by the adiabatic 6 $^1\Sigma^+$ potential (dashed line) and the adiabatic 7 $^7\Sigma^+$ potential (chain line).

to $t=0$. The same process repeats until t exceeds $\sim$55 a.u. To examine whether this rapid oscillation is a real physical phenomenon or an artifact of the choice of the basis set, we transformed the 6 $^1\Sigma^+$ and 7 $^1\Sigma^+$ wave functions, and the relevant potentials and coupling matrix elements to the diabatic representation [17]. Figure 7 shows the process of this transformation. From the radial coupling matrix elements between 7 $^1\Sigma^+$ and 6 $^1\Sigma^+$ shown in Fig. 7(a), we calculate $\omega(R)$ [full line in Fig. 7(b)], $\sin\omega(R)$ [dotted line in Fig. 7(b)] and $\cos\omega(R)$ [dot-dashed line in Fig. 7(b)]. Then the diabatic potentials given by

$$E_{6\Sigma,dia}(R) = E_{6\Sigma,adia}(R)\cos^2\omega(R) + E_{7\Sigma,adia}(R)\sin^2\omega(R),$$
$$E_{7\Sigma,dia}(R) = E_{6\Sigma,adia}(R)\sin^2\omega(R) + E_{7\Sigma,adia}(R)\cos^2\omega(R) \quad (4)$$

are shown in Fig. 7(c), together with the adiabatic potentials of 6 $^1\Sigma^+$ and 7 $^1\Sigma^+$ potentials. The diabatic potential curves are always inside the two adiabatic 6 $^1\Sigma^+$ and 7 $^1\Sigma^+$ potential curves, and they cross each other near the avoided crossings. The potential coupling term given by

$$[E_{6\Sigma,adia}(R) - E_{7\Sigma,adia}(R)]\sin\omega(R)\cos\omega(R) \quad (5)$$

is too small to show in this figure. This transformation eliminates the coupling between 6 $^1\Sigma^+$ and 7 $^1\Sigma^+$, and replaces it by the potential coupling. Though the magnitude of this potential coupling is weak, it is oscillatory because of the coefficients. Other coupling matrix elements involving the adiabatic 6 $^1\Sigma^+$ and 7 $^1\Sigma^+$ are also transformed to the diabatic representation, which involves again the sinusoidal coefficients of $\omega(R)$. Using this diabatic representation, we repeated the same calculations. The diabatic result is shown by the full line in Fig. 6(b). The oscillation of the probability of the 7 $^1\Sigma^+_{dia}$ is greatly reduced, but is nonvanishing. Also, we notice that, for example, if we compare the time evolution of the probability of the 4 $^1\Pi^+$ state shown by the dotted lines in Figs. 6(a) and 6(b), the nonoscillatory behavior in the adiabatic representation in Fig. 6(a) changed to a rapidly oscillating one in Fig. 6(b). Similar trends were observed in other diabatic states. This kind of rapid oscillation was seen in plots of the time variation of the wave functions in a Xe Rydberg atom colliding with a metal surface [18]. The contour plots of the electron probability densities of the states near the avoided crossing in their paper show rapid changes. Whether the electron probability densities of the *individual* states in a particular representation show similar rapid changes depends on the choice of the basis set. However, we believe that the rapid change of the net sum of the electron probability near the avoided crossing is a physical effect.

Finally, we estimate the uncertainty of the calculated charge-transfer cross sections. The main source of possible errors to the magnitude of the charge-transfer cross sections comes from the long-range interaction ($R\sim17$ a.u.) between the 6 $^1\Sigma^+$ and 7 $^1\Sigma^+$ states. The rough estimate of the size of the interaction at this point is inversely proportional to the product of the energy gap ΔE between these states, and interacting region a. If ΔE is reduced by a factor of 2, this will double the size of the interaction, although since a and ΔE tend to change in the opposite directions, the product of the two will not change as much as a change of ΔE alone. We also expect that the radial coupling matrix elements peak more as the energy gap decreases. Therefore, decrease of the energy gap tends to increase the interaction. Although we consider that the 6 $^1\Sigma^+$ and 7 $^1\Sigma^+$ states we obtained are reasonably accurate for the chosen core potential Eq. (2), our STO basis set is not complete. Since the partial charge-transfer cross sections to 7 $^1\Sigma^+$ are about 47% of the total charge-transfer cross sections, and the contribution beyond $b=10$ a.u. to the 7 $^1\Sigma^+$ partial charge-transfer cross sections is about 47%, we estimate the net error from the avoided crossing near $R=17.23$ a.u. to be $\sim$25%. The 4 $^1\Pi^+$ partial cross section, which contributes comparable amounts to the total charge-transfer cross section, will be also indirectly affected by this avoided crossing. The contribution from b larger than 10 a.u. is about 70%. Since the effect of ΔE is indirect, we estimate this error to be $\sim$20%. The convergence criterion we used for solving iteratively the coupled differential equations for the amplitudes is that the amplitudes of all channels at $t=\infty$ should converge within 2%. Compared with the convergence criterion of 5%, the probabilities of the individual channels agreed to three effective digits. Other sources of error are inaccuracies in all the molecular potentials, wave functions, and resulting coupling matrix elements caused by the pseudopotential for the core electrons of Ca, optimization of STO exponents at a finite distance ($R=30$ a.u., which we believe far enough), and the limited STO basis set. We estimate this error to be $\sim$15%. Therefore, we estimate the overall uncertainty of the calculated cross sections to be about 60%. To further improve the accuracy using the molecular-orbital close-coupling method, we would require a much larger, near-complete basis set as well as avoiding the pseudopotential for the core electrons. This will require formidable calculations, pushing the method to the limit. Some alternate approaches may be more appropriate.

IV. CONCLUSION

We have calculated cross sections for charge transfer in collisions of H^+ and $Ca(4s^2)$, at center-of-mass collision energies ranging from 200 eV/u to 10 keV/u of collision energy. We used the molecular-orbital coupling method, together with the semiclassical straight-line impact-parameter approximation. Inclusion of the Ca^{2+}-H^- configurations in the configuration-interaction calculations of the molecular orbital is crucial and it creates many narrow avoided crossings, which otherwise do not appear. Because of the avoided crossings at large internuclear separations, the charge transfer is a long-range phenomenon, in contrast to the short range in most collision systems so far studied. The relevant molecular states in charge transfer are highly excited states, and at present there are no theoretical and experimental data to compare and examine the goodness of our wave functions and potentials for those excited states at large internuclear separations. The calculated total charge-transfer cross sections vary monotonically from 3.4×10^{-15} cm^2 at 200 eV/u to 4.5×10^{-15} cm^2 at 10 keV/u. In the entire energy range, charge transfer to $Ca^+(5p)$, which is the sum of the partial charge-transfer cross sections for $7\,^1\Sigma^+$ and $1\,^1\Pi$, dominates, yielding close to 47% of the total cross section at 200 eV/u and 38% at 10 keV/u. The contributions from $7\,^1\Sigma^+$ and $1\,^1\Pi$ to generation of $Ca^+(5p)$ ion are almost equal in magnitude in the entire energy range. This is followed by charge transfer to $Ca^+(4d)$, which is the sum of the contributions from $5\,^1\Sigma^+$ and $3\,^1\Pi$. The $5\,^1\Sigma^+$ and $3\,^1\Pi$ states lie just below the incoming channel. The transfer to $Ca^+(4d)$ increases with the collision energy, and becomes of the same magnitude as that of $Ca^+(5p)$, each contributing ~38% to the total cross section at 10 keV/u. The higher excited states leading to production of $Ca^+(6s)$, $Ca^+(5d)$, and $Ca^+(6p)$ give less than 9% of the total charge-transfer cross sections in the entire energy range. The main source of possible error is the accuracy of the energy gap at the avoided crossing at the internuclear separation of 17.23 a.u. between the incoming $6\,^1\Sigma^+$ state and the energetically nearly degenerate $7\,^1\Sigma^+$ state. Combining with errors from other sources, we estimate the overall uncertainty of the calculated total cross sections to be roughly 60%. More accurate calculations will require a much larger nearly complete basis set, without using a pseudopotential for the core electrons. However, this will lead to formidable calculations, if one uses the present method.

ACKNOWLEDGMENTS

The research was supported in part by a Grant in Aid, Ministry of Education, Science and Culture, Japan and The Japan Society for Promotion of Science, and a grant to the Institute for Theoretical Atomic and Molecular Physics at Harvard University and Smithsonian Astrophysical Observatory (M.K.), by the Robert A. Welch Foundation under Grant No. C-1222, by the National Science Foundation through Grant No. INT-9911858 (PN,CMD), and by the Chemical Sciences, Geosciences and Biosciences Division of the Office of Basic Energy Sciences and the Department of Energy (A.D.).

[1] P. C. Frisch, Space Sci. Rev. **72**, 499 (1995).
[2] D. E. Welty, D. C. Morton, and L. M. Hobbs, Astrophys. J., Suppl. Ser. **106**, 533 (1996).
[3] S. Redfield and J. L. Linsky, Astrophys. J., Suppl. Ser. **139**, 439 (2002).
[4] E. L. Lewis, L. F. McNamara, and H. H. Michels, Phys. Rev. A **3**, 1939 (1971).
[5] T. S. Monteiro, A. S. Dickinson, and E. L. Lewis, J. Phys. B **18**, 3499 (1985).
[6] T. S. Monteiro, G. Danby, I. L. Coper, A. S. Dickinson, and E. L. Lewis, J. Phys. B **21**, 4165 (1988).
[7] J. L. Lemaire, J. L. Chotin, and F. Rostas, J. Phys. B **18**, 95 (1985).
[8] G. Smith, T. S. Monteiro, A. S. Dickinson, and E. L. Lewis, Mon. Not. R. Astron. Soc. **217**, 679 (1985).
[9] C. Richter, N. Andersen, J. C. Brenot, D. Dowek, J. C. Houver, J. Salgado, and J. W. Thomsen, J. Phys. B **26**, 723 (1993).
[10] M. Kimura and W. R. Thorson, Phys. Rev. A **24**, 3019 (1981).
[11] A. Dalgarno, Adv. Phys. **11**, 281 (1962).
[12] M. Kimura, H. Sato, and R. E. Olson, Phys. Rev. A **28**, 2085 (1983).
[13] C.-T. Lin and C. S. G. Lee, *Neural Fuzzy Systems: A Neuro-Fuzzy Synergism to Intelligent Systems* (Prentice-Hall, Englewood Cliffs, NJ, 1996).
[14] C. E. Moore, *Atomic Energy Levels*, Natl. Bur. Stand. (U.S.) Circ. No. 467 (U.S.T.P.O, Washington, DC, 1971).
[15] B. Kerkeni, A. Spielfiedel, and N. Feautrier, Astron. Astrophys. **402**, 5 (2003).
[16] A. Boutalib, J. P. Daudey, and M. El Mouhtadi, Chem. Phys. **167**, 111 (1992).
[17] T. G. Heil, S. E. Butler, and A. Dalgarno, Phys. Rev. A **23**, 1100 (1981).
[18] C. Oubre, P. Nordlander, and F. B. Dunning, J. Phys. Chem. B **106**, 8338 (2002).
[19] M. I. Chibisov and R. K. Janev, Phys. Rep. **166**, 1 (1988).